



Article

Deep Learning-Based System for Early Symptoms Recognition of Grapevine Red Blotch and Leafroll Diseases and Its Implementation on Edge Computing Devices

Carolina Lazcano-García ¹, Karen Guadalupe García-Resendiz ², Jimena Carrillo-Tripp ², Everardo Inzunza-Gonzalez ¹, Enrique Efrén García-Guerrero ¹, David Cervantes-Vasquez ¹, Jorge Galarza-Falfan ¹, Cesar Alberto Lopez-Mercado ¹ and Oscar Adrian Aguirre-Castro ^{1,*}

¹ Facultad de Ingeniería Arquitectura y Diseño, Universidad Autónoma de Baja California, Carrt. Tijuana-Ensenada No. 3917, Ensenada 22860, Baja California, Mexico; lazcano.carolina@uabc.edu.mx (C.L.-G.); einzunza@uabc.edu.mx (E.I.-G.); eegarcia@uabc.edu.mx (E.E.G.-G.); dcervantes42@uabc.edu.mx (D.C.-V.); jorge.galarza@uabc.edu.mx (J.G.-F.); lopez.cesar7@uabc.edu.mx (C.A.L.-M.)

² Departamento de Microbiología, Centro de Investigación Científica y de Educación Superior de Ensenada, Baja California (CICESE), Ensenada 22860, Baja California, Mexico; karengg@cicese.edu.mx (K.G.G.-R.); jcarrillo@cicese.mx (J.C.-T.)

* Correspondence: oscar.aguirre@uabc.edu.mx



Academic Editors: Francesco Marinello, Yee Siang Gan and Sze-Teng Liong

Received: 6 December 2024

Revised: 30 January 2025

Accepted: 21 February 2025

Published: 3 March 2025

Citation: Lazcano-García, C.; García-Resendiz, K.G.; Carrillo-Tripp, J.; Inzunza-Gonzalez, E.; García-Guerrero, E.E.; Cervantes-Vasquez, D.; Galarza-Falfan, J.; Lopez-Mercado, C.A.; Aguirre-Castro, O.A. Deep Learning-Based System for Early Symptoms Recognition of Grapevine Red Blotch and Leafroll Diseases and Its Implementation on Edge Computing Devices. *AgriEngineering* **2025**, *7*, 63. <https://doi.org/10.3390/agriengineering7030063>

Copyright: © 2025 by the authors. Licensee MDPI, Basel, Switzerland. This article is an open access article distributed under the terms and conditions of the Creative Commons Attribution (CC BY) license (<https://creativecommons.org/licenses/by/4.0/>).

Abstract: In recent years, the agriculture sector has undergone a significant digital transformation, integrating artificial intelligence (AI) technologies to harness and analyze the growing volume of data from diverse sources. Machine learning (ML), a powerful branch of AI, has emerged as an essential tool for developing knowledge-based agricultural systems. Grapevine red blotch disease (GRBD) and grapevine leafroll disease (GLD) are viral infections that severely impact grapevine productivity and longevity, leading to considerable economic losses worldwide. Conventional diagnostic methods for these diseases are costly and time-consuming. To address this, ML-based technologies have been increasingly adopted by researchers for early detection by analyzing the foliar symptoms linked to viral infections. This study focused on detecting GRBD and GLD symptoms using Convolutional Neural Networks (CNNs) in computer vision. YOLOv5 outperformed the other deep learning (DL) models tested, such as YOLOv3, YOLOv8, and ResNet-50, where it achieved 95.36% Precision, 95.77% Recall, and an F1-score of 95.56%. These metrics underscore the model's effectiveness at accurately classifying grapevine leaves with and without GRBD and/or GLD symptoms. Furthermore, benchmarking was performed with two edge computer devices, where Jetson NANO obtained the best cost–benefit performance. The findings support YOLOv5 as a reliable tool for early diagnosis, offering potential economic benefits for large-scale agricultural monitoring.

Keywords: grapevine; red blotch disease; leafroll disease; preventive diagnosis; artificial intelligence; computer vision; CNN; deep learning; ResNet; YOLO

1. Introduction

In recent years, the agricultural sector has undergone a significant digital transformation, incorporating artificial intelligence (AI) technologies to harness and effectively analyze the increasing volume of data from diverse sources and extract valuable insights. In the context of artificial intelligence (AI), machine learning (ML) is recognized as a powerful tool for addressing the many challenges associated with developing knowledge-based agricultural

systems [1]. Furthermore, the global vineyard area in 2022 was estimated to span 7.3 million hectares, with approximately 258 million hectoliters of wine produced worldwide during that same year [2]. In Mexico, 36,586.5 hectares are dedicated to grape cultivation [3], including approximately 80 grape varieties, with 50% of this area designated for industrial purposes, primarily wine production [4]. Baja California is an important viticulture region that has seen exponential growth in recent years, covering an estimated 4365 hectares [5]. Between 2016 and 2017, grapevine plant samples that exhibited GRBD symptomatology were collected in Ensenada, Baja California, as shown in Figure 1. These samples were analyzed using polymerase chain reaction (PCR) and were found to be positive for grapevine red blotch virus (GRBV), the causative agent of GRBD [6,7]. GRBV belongs to the Grablovirus Vitis species in the Geminiviridae family. Similar to other geminiviruses, GRBV has a single-stranded DNA genome encapsidated in a geminate particle [8,9]. GRBV is spread by the three-cornered alfalfa hopper *Spissistilus festinus* and through the propagation of infected material [10]. Moreover, other viruses can infect grapevines and even co-infect them. Specifically, grapevine leafroll-associated viruses (GLRaVs), such as grapevine leafroll-associated virus 1 (GLRaV-1), grapevine leafroll-associated virus 2 (GLRaV-2), and grapevine leafroll-associated virus 3 (GLRaV-3), can cause symptoms of GLD, as depicted in Figure 1a,c,d,h. GLRaVs belong to the Closteroviridae family [11] and are transmitted by infected plant material and vectors, such as several species of mealybugs and scales [12]. The grapevine mealybug *Planococcus ficus* particularly affects Baja California and is one of the primary vectors of GLRaV-3 [13,14], as well as coccoids, such as *Pulvinaria vitis*, *Parthenolecanium corni*, *Ceroplastes rusci*, and *Coccus longulus* [15]. In the past two decades, GLD has emerged as a significant threat to grapevine production, leading to an estimated 60% reduction in yield and a decline in grape quality [16].

GLD severely affects vine vigor and physiology, leading to uneven ripening and reduced yield and berry quality due to lower sugar content [17,18]. GRBV-infected grapevine plants show significant physiological disorders, such as changes in metabolism, accumulation of starch and soluble sugars, and a decrease in photosynthesis [19]; consequently, there is an inhibition of the ripening pathways, impacting the concentrations of sugar, phenolic, and volatile compounds in whole grapes and wines [20,21]. GRBD and GLD viruses disrupt the plant physiology and metabolism, negatively impacting vineyard profits by reducing fruit quality and ripening, resulting in estimated economic losses ranging from USD 2213 to 68,528 [22].

When GRBV infects a grapevine plant, the virus causes symptomatology comprising irregular red spots on the leaves, especially on the edges, reddish colored veins, and irregular edges [23], as seen in Figure 1b,c,e–h. It should be noted that GRBV infects a wide range of white-berry cultivars (Chardonnay, Riesling, Sauvignon blanc, etc.) and red-berry cultivars (Cabernet Franc, Cabernet Sauvignon, Malbec, Merlot, Mourvèdre, Petit Verdot, Petite Syrah, Pinot noir, Zinfandel, etc.) [8]. For their part, GLRaVs can potentially affect a large number of wine grape varieties; however, red-berry cultivars usually present the most characteristic foliar symptoms of the disease, comprising red and reddish-purple discolorations, and these expand over time, showing a downward rolling of the leaves at the end of the annual physiological cycle [24]. GRBD and GLD share the symptom of red blotchiness in specific spots or the entire leaf bundle. Initially, GLRaV was thought to cause GRBV symptoms [25].

GRBD was first identified in 2008 as a disease affecting grape production. To enhance the detection and monitoring of the virus, ref. [26] developed a method for sample processing and a multiplex polymerase chain reaction assay. This development was prompted by observing symptoms that resembled GLD in an 8-year-old Cabernet Sauvignon vineyard at the experimental research station of the Department of Viticulture and Enology at the Uni-

versity of California [25]. Although molecular diagnosis remains the most reliable method for detecting viruses, leaf symptomatology can approximate the presence of grapevine diseases. Therefore, it is feasible to use AI to efficiently classify grapevine leaves according to the presence or absence of GRBD and GLD symptoms indistinctly, enabling the diagnosis of these viruses through digital images. According to refs. [8,27], GRBD and GLD symptoms are recurrent in various regions, suggesting that the presence or absence of symptoms is not strictly determined by geographic location. Instead, symptom expression is primarily differentiated between red and white cultivars [28]. While climate and geographic factors may influence the stage of vegetative development in which symptoms manifest and their severity during the annual cycle [29], they do not dictate whether symptoms will appear. Therefore, DL models can be adapted using techniques such as transfer learning to enhance their classification performance across different datasets and conditions. This work compared the results of CNN models, such as YOLOv3, YOLOv5, YOLOv8, and ResNet-50. Among these, YOLOv5 achieved the best detection performance, with a 95.36% Accuracy, using a new dataset of 3198 images supported by 800 images of molecular diagnostics. Furthermore, benchmarking was performed with two edge computing devices, where Jetson Nano (NVIDIA Corporation, Santa Clara, CA, USA) obtained the best cost–benefit performance. The best-performing model was integrated into a graphical user interface (GUI) for the inspection of images, video, and real-time video in the field and laboratory.

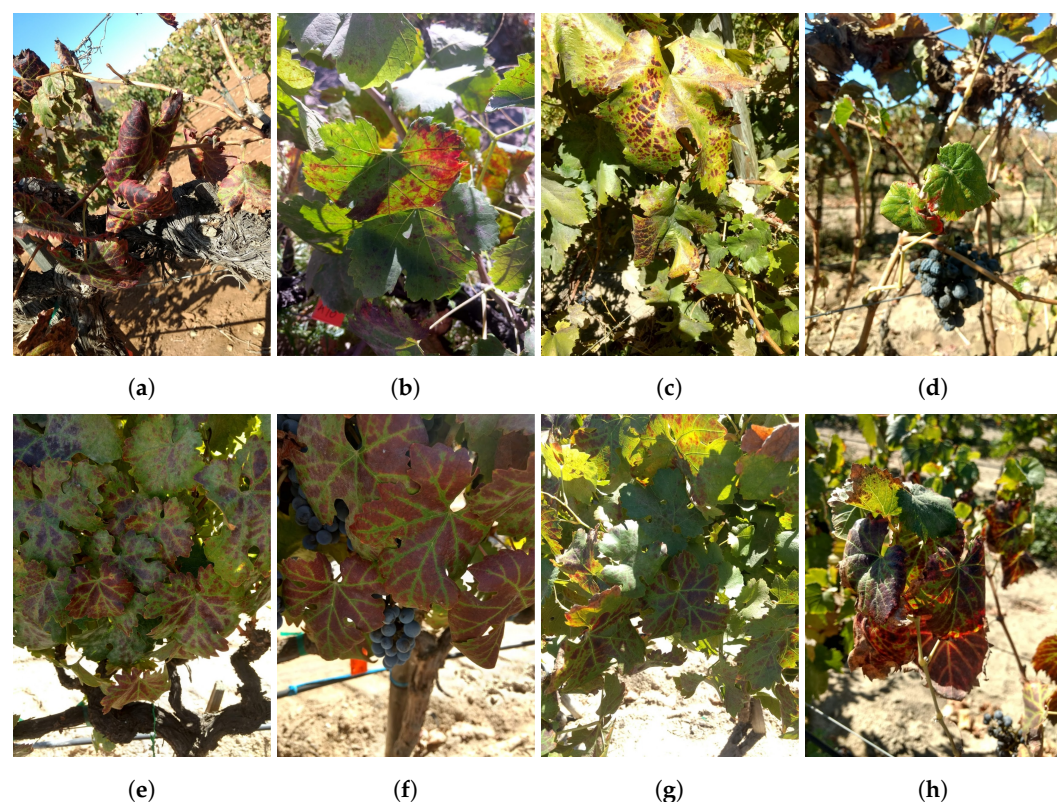


Figure 1. Grapevine plants with GRBD and/or GLD symptoms: (a) plant with GLRaV-3 and GRBV symptoms exhibiting irregular red spots on leaves, light green veins, and margin rolling; (b) grapevine plant with GLRaV-1 symptoms exhibiting red pixelated blotches; (c) grapevine plant with GLRaV-2 and GRBV symptoms comprising red pixels on the leaf and margin rolling; (d) grapevine plant with GRBV symptoms, with red pixelated blotches on the margin; (e–g) grapevine plant with GLRaV-3 symptoms, exhibiting red blotches and light green veins; (h) grapevine plant with GLRaV-3 and GRBV symptoms, presenting irregular red spots on the leaves, light green veins, and margin rolling.

The structure of the following sections is as follows: Section 2 contains information on recent related research; Section 3 presents the proposed method and materials; Section 4

presents the obtained results; Section 5 discusses the results compared with related work; and lastly, Section 6 presents the conclusions.

2. Related Work

New methods based on AI technologies garnered significant interest in scientific research for grapevine disease management. The medicinal leaf detection model based on P-Net, S-Net, and R-Net architectures, developed by [30], achieved accuracies above 97% when evaluated across three distinct datasets, thereby illustrating its generalizability. Nevertheless, the authors emphasized the importance of handling environmental factors, particularly the potentially poor quality of leaf images and changing lighting conditions. Furthermore, they intended to explore alternative DL architectures to enhance the performance of the computer vision system for its use in the field. The authors of [1] highlighted the high Accuracy and efficiency of CNNs in grapevine diagnosis, although they noted the limited availability of accessible image datasets for grapevine diseases. Complementarily, refs. [17,31] employed hyperspectral imaging and achieved Accuracies between 66.67% and 89.93%. They also utilized reverse transcription polymerase chain reaction (RT-PCR) for molecular diagnosis and identified characteristic wavelengths of 690, 715, 731, 1409, 1425, and 1582 nm as critical for the early detection of GLD. These studies demonstrated that hyperspectral imaging is effective for the non-destructive detection of grapevines infected with GLD. Authors [32] used the AlexNet architecture to train a dataset of 40,000 images of healthy and diseased leaves. The developed detection system successfully identified nine plant species and 24 diseases with an Accuracy of 98.90%. In [33], the authors performed a diagnostic detection of grape diseases using various CNN and Transformer vision models. Four models achieved 100% Accuracy using a dataset of Plant Village 4062 images. In [34], a dataset of 295 images was utilized across seven classifier models, which reached an Accuracy of 96%. In [31], diagnostic efforts with ML models, such as Random Forest (RF), and a CNN model that used 500 hyperspectral images reported an Accuracy of 87%. For grape cluster detection and physical grape injury assessment, ref. [35] employed CNN models with a dataset of 910 images, where YOLOv7 achieved the highest Accuracy, approximately 98%. In [36], 15 grape diseases were identified with an improved CNN model, which obtained a 99.1% Accuracy. Ref. [37] conducted a comparison of deep learning models for vine growth stage recognition using three classifier models and reported that ResNet provided better results with a 88.1% Accuracy. Ref. [17] detected three viruses associated with GLD in an ML classifier using a least squares support vector machine with Accuracies that ranged from 66% to 89%. Table 1 summarizes and compares the articles reviewed with the results obtained in this work.

Table 1. Comparative analysis of DL classification methods for grapevine diseases.

Reference	Contributions	Algorithm/Model	Dataset	Results	Year
This work	Identification of symptoms related to GLD and GRBD in grapevines (<i>Vitis vinifera</i>)	DL, CNN and YOLOv5	3198 grapevine leaf images	YOLOv5 achieved an Accuracy of 95.36%, Overall Recall 95.77%, and F1-score 95.56%	2025
Kunduracioglu et al. [33]	Accurate classification of grapevine leaves and diagnosis of grape diseases	Performance comparison of 14 CNN and 17 vision Transformer models	4062 images from the PlantVillage dataset and 500 images from the Grapevine dataset	4 models reached an Accuracy of 100% for both datasets	2024
Elsherbiny et al. [34]	Rapid grapevine diagnosis using DL	CNN, LSTM, DNN, transfer learning with VGG16, VGG19, ResNet50, and ResNet101V2	295 images from the PlantVillage dataset	Validation Accuracy, Precision, Recall, and F1-score of 96.6% and an intersection over union of 93.4%	2024

Table 1. Cont.

Reference	Contributions	Algorithm/Model	Dataset	Results	Year
Sawyer et al. [31]	Detection of GLD and GRBD in grapevine leaves	RF and 3D CNN	500 hyperspectral images	The CNN model performed better, with an average Precision of 87% against 82.8% from the RF model	2023
Pinheiro et al. [35]	Grape bunch detection and identification of biophysical lesions	YOLOv5x6, YOLOv7-E6E, and YOLOR-CSP-X	910 images	YOLOv7 achieved the best results with a Precision of 98%, a Recall of 90%, an F1-score of 94%, and a mAP of 77%	2023
Wang et al. [36]	Identification of 15 grape diseases	Improved YOLOXS and Convolutional Block Attention Module (CBAM)	China State Key Laboratory of Plant Pest Biology dataset	Average Precision of 99.1%	2023
Schieck et al. [37]	Grapevine growth stage recognition using DL models	ResNet, DenseNet, and InceptionV3	Grapevine growth stage dataset (BBCH 71-79)	ResNet achieved the best classification results with an average Accuracy of 88.1%	2023
Gao et al. [17]	Identification of GLRaV-3 virus during asymptomatic and symptomatic stages of GLD	Least squares support vector machine (LS-SVM)	500 hyperspectral images	Classifier Precision between 66.67% and 89.93%	2020

3. Materials and Methods

This section provides details on the equipment used for the leaf molecular diagnosis; the hardware and software tools required to perform the advanced image classification; and, ultimately, a GUI-based implementation of the model validated with images taken directly from the vineyard to evaluate the reliability of the proposed methodology.

Consequently, the trained DL model in this study was tested in three different hardware devices to select the best option considering their performance and the requirements of the use scenario. Table 2 comprises the characteristics of the three tested devices: NVIDIA Jetson Nano (NVIDIA Corporation, Santa Clara, CA, USA), Raspberry Pi 4 (Raspberry Pi Foundation, Cambridge, UK), and a laptop hp victus d15 (Hewlett-Packard Company, Palo Alto, CA, USA).

Table 2. Summary of the main characteristics of the three edge computing devices tested: a personal computer (laptop), NVIDIA Jetson Nano, and Raspberry Pi 4.

Edge Computing Device	CPU	GPU	RAM	Cost [USD]
Personal computer (laptop)	Ryzen 7 5800H	RTX 3050	40 GB	1000.00
Jetson Nano	Quad-core ARM Cortex-A57	128-core Maxwell	2 GB LPDDR4	149.00
Raspberry Pi 4	Quad-core ARM Cortex-A72	Broadcom VideoCore VI	4 GB LPDDR4	72.80

The procedure shown in Figure 2 began with data collection, which included gathering grapevine leaf samples and capturing digital images of each sample to create an annotated dataset for DL image classification. The second phase involved preparing the data for DL model training, which included balancing the classes, selecting, training, validating the DL model based on the literature review, and choosing the most appropriate performance metrics to evaluate the model according to the project's priorities. The third phase consisted of running the trained model in inference mode on three computing devices. Finally, a real-world use scenario for the DL-based grapevine leaf disease detector is proposed.

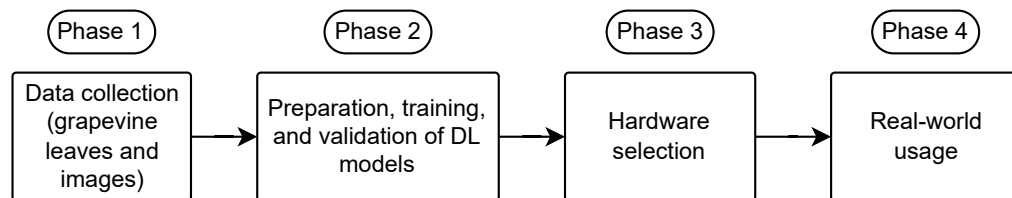


Figure 2. Methodology for sample collection and classification.

3.1. Data Collection

The sample collection of *Vitis vinifera* L. was conducted following the UC-Davis Foundation Plant Services guidelines [38], with modifications requiring the collection of at least 10 leaves and transportation in coolers with refrigerant gels. All vineyard owners or their representatives signed an informed consent form to participate in the project. To ensure data confidentiality, the identity and exact location of the sampled vineyards are not disclosed. The data collection methodology is detailed in Figure 3. For the leaf sampling, between 5 and 10 leaves were photographed from each plant, totaling 360 plants sampled throughout Baja California. The collections were carried out during October (the peak period for symptom manifestation) from 2018 to 2019 and from 2021 to 2023 [39]. The leaves were selected from various sections of each plant (top, bottom, right, left, and center) to include young and mature leaves that displayed diverse symptomatology. The field-collected samples were transported to the Agricultural Virology Laboratory at CICESE in airtight bags with cooling gels. Molecular diagnostics were conducted on several leaves to confirm the presence or absence of viruses associated with GRBD and GLD, and to correlate leaf symptoms with the amplification of genomic regions of GRBV and GLRaVs (GLRaV-1, GLRaV-2, GLRaV-3, and GLRaV-4). The total nucleic acids were extracted following the protocol of [40] with modifications, and real-time RT-PCR was performed according to the protocols [26,41], with modifications using EvaGreen dye.

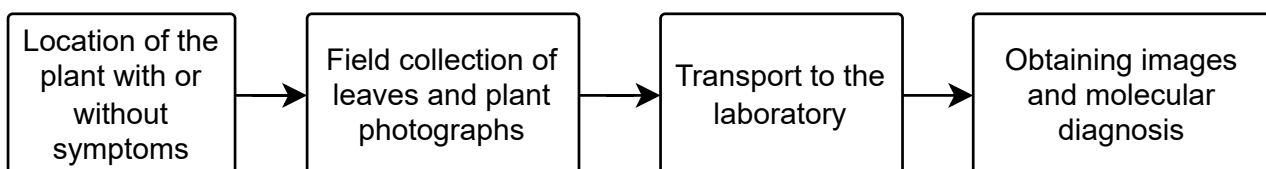


Figure 3. Methodology for data collection.

Individual leaf images were captured using conventional smartphone cameras, with specifications provided in Table 3. Photographs were taken under natural and artificial lighting, using lamps to enhance the leaf features and color details. After obtaining laboratory diagnostic results, grapevine plants with confirmed viral infections were photographed in the field. The dataset composition (Table 3) included 0.3% of images collected in 2018 (four cultivars), 0.4% in 2019 (eight cultivars), 35.7% in 2021 (four cultivars), 32.6% in 2022 (thirteen cultivars), and 30.9% in 2023 (thirteen cultivars). Notably, 43.3% and 35% of the leaves photographed in 2022 and 2023, respectively, underwent molecular diagnostics.

Images of individual leaves were captured using conventional smartphone cameras, which had the characteristics detailed in Table 4. These photographs were taken under natural and artificial lighting, using lamps to highlight the characteristics of the leaves, which enhanced the details and colors. Additionally, after obtaining the laboratory test results, grapevine plants with verified virus symptoms were photographed in the field.

Table 3. Conformation of the dataset according to the year of obtaining, grapevine cultivar, and molecular diagnosis.

Year	Number of Images	Grapevine Cultivar	Leaves with Molecular Diagnosis Photographed
2023	989	Tempranillo, Syrah, Cabernet Sauvignon, Malbec, Nebbiolo, Barbera, Chenin blanc, Thompson, Crimson, Grenache, Red globe, Sauvignon blanc, and Mision	347
2022	1044	Tempranillo, Syrah, Cabernet Sauvignon, Chenin blanc, Colombard, Malbec, Nebbiolo, Merlot, Chardonnay, Grenache, Red globe, Carignan, and Petite Syrah	453
2021	1142	Cabernet Sauvignon, Nebbiolo italiana, Merlot, and Nebbiolo	0
2019	13	Gamay, Nebbiolo, Mounedre, Petit verdot, Merlot, Cabernet Sauvignon, Mision, and Crimson	0
2018	10	Nebbiolo, Temporal, Chardonnay, and Tempranillo	0
Total	3198	23 different cultivars	800

Table 4. Characteristics of the cellphones' cameras used for image acquisition.

Model	Resolution	Wide Angle Aperture	Ultra-Wide Angle Aperture	Telephoto Lens	Image Format
iPhone 8	12 MP	f/1.8	NA	NA	HEIF and JPEG
iPhone 10	12 MP	f/1.8	NA	f/2.4 lens aperture	HEIF and JPEG
iPhone 13	12 MP	f/1.6	f/2.4 lens aperture, 120° field of view	NA	HEIF and JPEG
iPhone 14	12 MP	f/1.5	f/2.4 lens aperture, 120° field of view	NA	HEIF and JPEG

3.2. DL Models Training

Before starting the training process for the DL models, it was essential to confirm that the dataset contained sufficient images to accurately detect the grapevine leaf disease symptoms. To address this, the diagram in Figure 4 illustrates an iterative process of image selection, training, and testing using the YOLOv5 model.

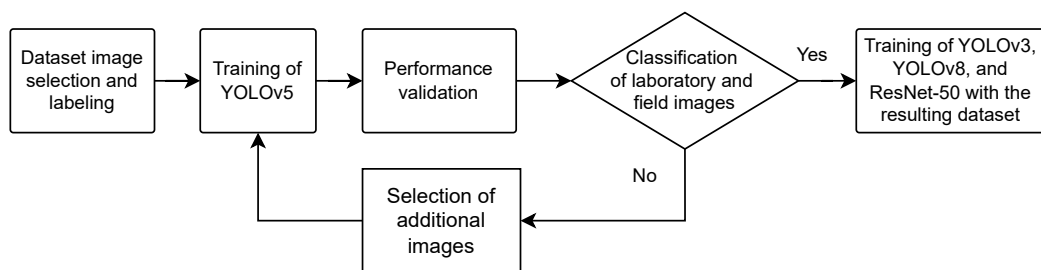
**Figure 4.** Data selection for training considering environment conditions.

Figure 5 shows in an illustrative manner how YOLOv5 focuses its attention and detects grapevine leaf diseases by processing images step by step. First, the Backbone extracts important details, like texture changes and patterns that might indicate disease. Then, the Neck combines information from different layers, helping the model recognize symptoms, even when lighting changes, leaves overlap, or parts of the image are blocked. Finally,

the Head makes the final predictions, identifying and locating diseased areas [42]. This architecture offers more stable detection for objects of different sizes and scales, lighting conditions, and rotation compared with previous versions [43].

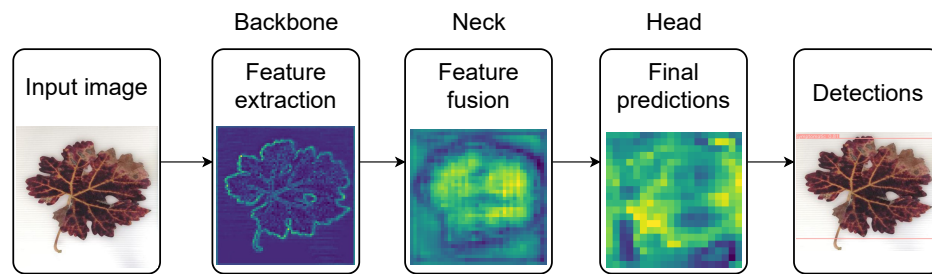


Figure 5. YOLOv5 architecture used to detect the grapevine diseases' key features.

Table 5 provides a clear and concise summary of the key hyperparameters used to train the YOLOv5 model. It includes parameters such as the image size (416×416), batch size (5), number of epochs (30), data configuration file, and pre-trained weights (`yolov5s.pt`). The learning rate (0.01) and the default optimizer (SGD) were also specified, highlighting the model's setup for efficient training. Additionally, Table 5 outlines the use of caching for faster data processing and deployment on a GPU-enabled device. Data augmentation is crucial for enhancing the generalization capability of deep learning models, particularly in object detection tasks. In YOLOv5, several augmentation hyperparameters are employed to improve the model robustness. The HSV Hue (0.015), Saturation (0.7), and Value (0.4) modified the color properties to simulate various lighting conditions. The Translation (0.1) shifted objects within an image, while the Scale (0.5) resized them to enhance the scale invariance. The Flip left-right (0.5) introduced horizontal mirroring, which reduced bias in the object orientation. Finally, the Mosaic (1.0) combined four images to increase the training diversity, which allowed the model to learn from varied object placements and occlusions [44]. This detailed configuration ensured reproducibility and transparency in the experimental setup.

Table 5. YOLOv5 hyperparameter configuration.

Hyperparameter	Value
Image size (-img)	416
Batch size (-batch)	5
Number of epochs (-epochs)	30
Data configuration file (-data)	<code>data.yaml</code>
Pre-trained weights (-weights)	<code>yolov5s.pt</code>
Experiment name (-name)	<code>yolov5s_results_EN</code>
Device (-device)	1
Cache images (-cache)	Enabled
Learning rate	0.01 (default initial value)
Optimizer	SGD (Stochastic Gradient Descent)
Data Augmentation Hyperparameter	Value
HSV Hue	0.015
HSV Saturation	0.7
HSV Value	0.4
Translate	0.1
Scale	0.5
Flip left-right	0.5
Mosaic	1

Once the model detects the classes correctly across images of varying quality, three additional DL models were trained. The second object detector implemented in this study was YOLOv3. Since its release in 2018, this architecture has been extensively studied in computer vision research [45]. The CNN behind YOLOv3 is Darknet-53 and it contains multiple layers that extract features of various scales from the input image. The model's final layer generates bounding boxes and predicts the object class. For more details, see [45]. YOLOv8 was the third model selected in this study due to its improved features compared with YOLOv5. These improvements include better generalization, the addition of advanced algorithms for calculating bounding boxes, and enhanced performance metrics. Although it outperforms YOLOv5 and earlier versions, YOLOv8 is also slower in real-time object detection tasks. This approach enhances object detection in low-resolution images [46]. For more details, see [47]. Finally, the last CNN model considered for this research was ResNet-50 due to its potential advantages in employing an architecture different from Darknet. ResNet-50 is a residual network with a simpler structure that connects layers through skip connections, enhancing the training efficiency [48]. For more details, consult [49].

3.3. Hardware Selection

The third phase of the methodology involved evaluating the selected DL model on three devices, including a personal computer (laptop) and the NVIDIA Jetson Nano and Raspberry Pi 4 edge computing devices, as illustrated in Figure 6. The objective was to identify the most suitable hardware under the operational conditions of the grapevine leaf symptom detector, whether in a field or laboratory setting, considering the performance of the device and its cost, as seen in Table 2.

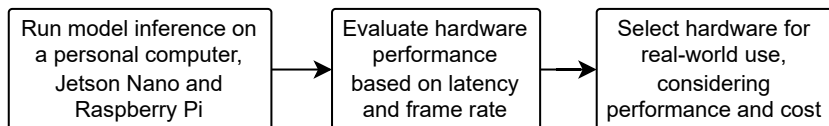


Figure 6. Selection of hardware for field and laboratory GDL and GRBD symptoms detection.

3.4. Real-World Usage

The last stage involved utilizing the predictions of the DL models in a graphic user interface (GUI), enabling users to upload and analyze new images or video recordings from the field or leaves brought to the laboratory, as depicted in Figure 7. Finally, the model classifies leaves as symptomatic or asymptomatic for GRBD and/or GLD with high probability, displaying the result in the GUI to provide a preventive diagnosis.

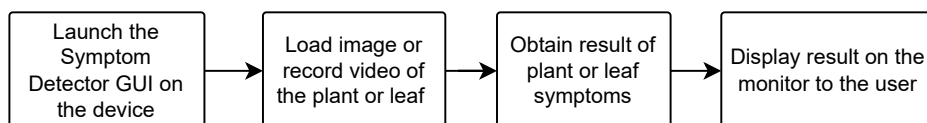


Figure 7. Methodology for using the model in the field or laboratory.

4. Results

This section presents the results obtained in this work, which involved collecting leaf samples from vineyards in Baja California and analyzing them using DL-based models to identify the most effective one and propose an implementation strategy.

4.1. Data Collection and Preparation

An asymptomatic leaf sample, examined using real-time RT-PCR, confirmed a positive diagnosis for the whole plant. A total of 800 leaf samples were analyzed using real-time RT-PCR. The outcome of this process was 3198 images, each of which was individually pho-

tographed. The categories for the diagnosis were *asymptomatic*, with a total of 1535 images for leaves with no symptoms of GLD or GRBD based on 200 images with real-time RT-PCR, and 1663 images in the *symptomatic* category for leaves that presented GLD and GRBD symptoms according to 600 images with real-time RT-PCR. Table 6 provides a summary of these results. The main symptoms observed on leaves classified as *symptomatic* were irregular red blotches in pixels (especially along the edges), reddish-colored veins, rolling of leaf edges and intense green veins. In contrast, asymptomatic leaves sometimes showed non-GRBD and GLD symptoms, such as edge wilting or necrosis, which were excluded from consideration in this work.

Table 6. Total of images in the dataset.

	Asymptomatic	Symptomatic	Total
RT-PCR diagnosis	200	600	800
Visual symptoms diagnosis	1335	1063	2398
Total	1535	1663	3198

The preparation of the dataset involved the second phase of the methodology (Figure 2) and included utilizing the image annotation tool Roboflow [50]. This tool was used to annotate images point by point, highlighting only the leaf to enhance its visual features and generate the dataset. After categorizing all the images, the classes were checked to ensure a balanced number of images in each class, thereby minimizing the risk of class imbalance, which could negatively impact the Accuracy of each class. Once the dataset was finalized, each DL model was coded and trained using Python. TensorFlow, Keras, and PyTorch were the libraries used to facilitate the implementation of the CNNs. The models were trained for 15 epochs using the dataset of 3128 images from the *symptomatic* and *asymptomatic* classes, as shown in Table 6.

Field images and new leaves were collected and taken to the laboratory to validate the trained model, ensuring the Accuracy percentages were suitable for presenting reliable results. The dataset included images under occlusion conditions, lighting fluctuations, obstacles, and overlapping, as observed in Figure 8. Several performance metrics, such as Precision, Accuracy, F1-score, and the confusion matrix, were used to evaluate the models. These metrics identified the DL model with the best performance for detecting GRBD and/or GLD symptoms.



(a)



(b)

Figure 8. Cont.

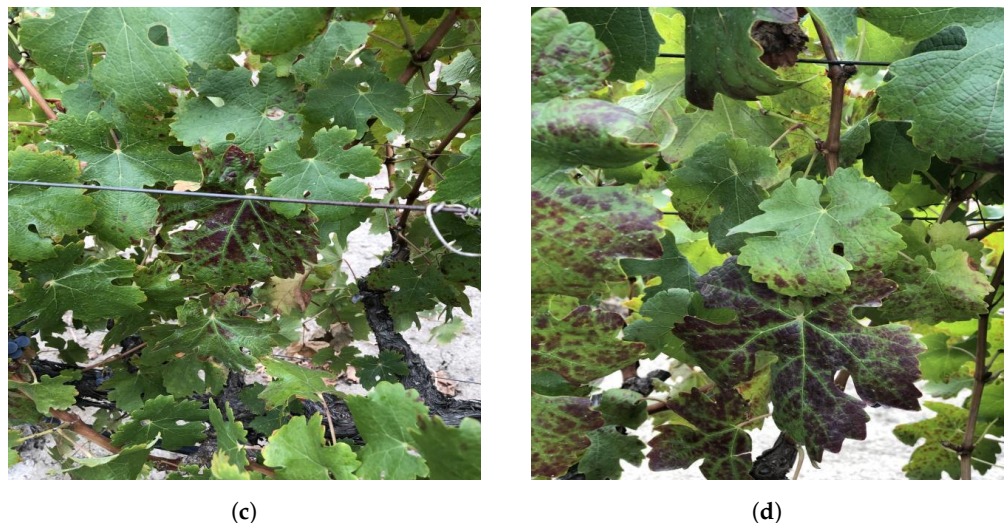


Figure 8. The dataset included the conditions (a) occlusion, (b) lighting fluctuations, (c) obstacles, and (d) leaf overlapping.

4.2. Training and Validation of DL Models

For YOLOv5, five different versions were trained to determine the optimal dataset size and balance between the number of images in the two classes to correctly detect and classify them, as illustrated in Figure 4. The first version included approximately 1000 images of asymptomatic leaves and over 1500 symptomatic leaves, organized as shown in Figure 9a.

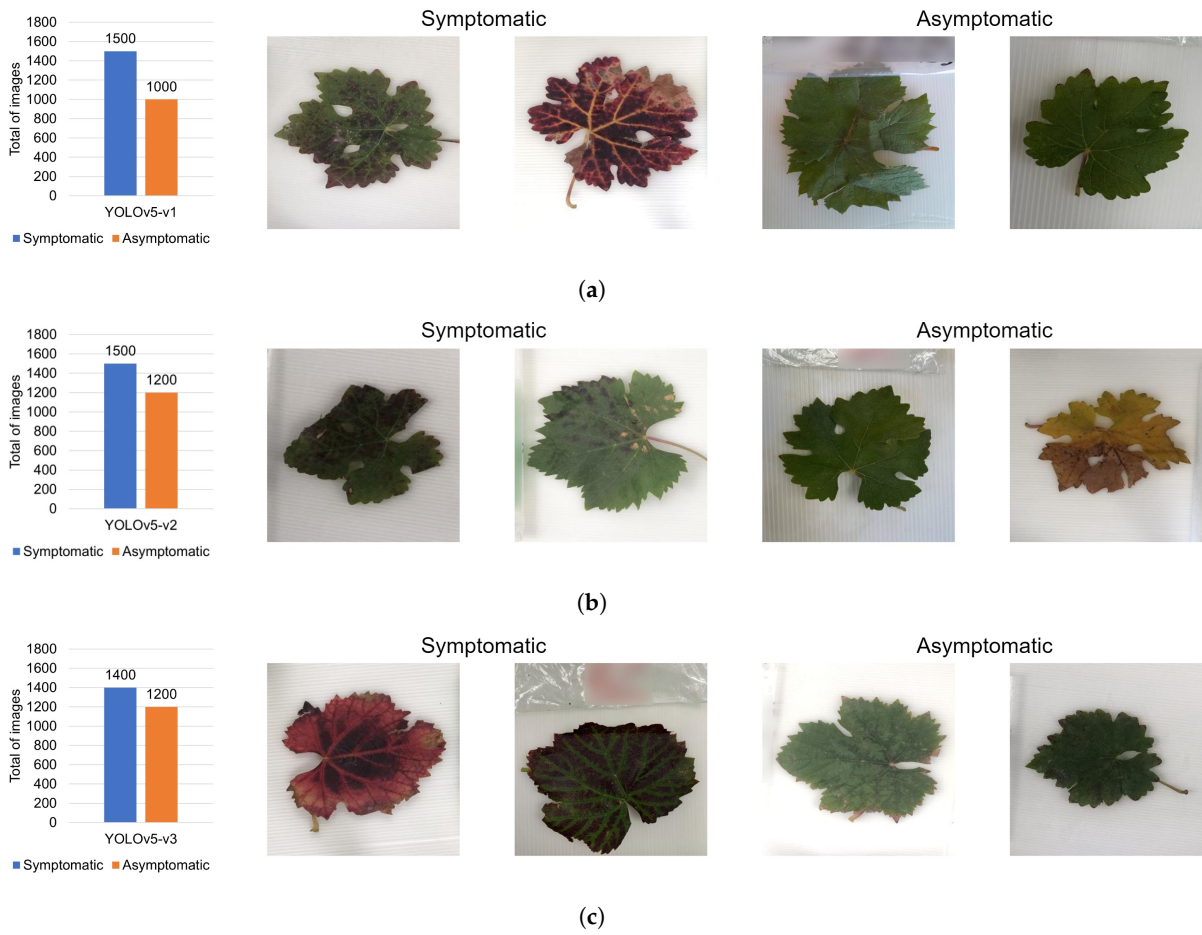


Figure 9. Cont.

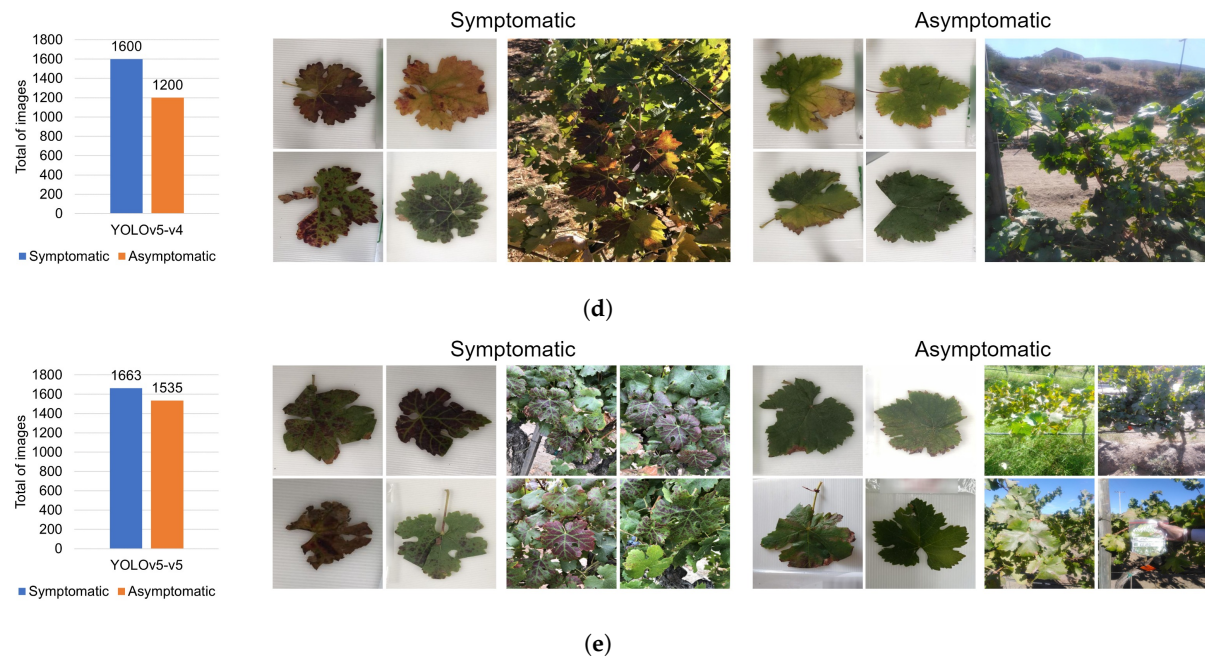


Figure 9. Total of images per class for the five versions of the model YOLOv5 (left), and visual features of the images in each class (right). (a) Classification of individual leaves for model YOLOv5-v1. (b) Classification of individual leaves for model YOLOv5-v2. (c) Classification of asymptomatic grapevine leaves for model YOLOv5-v3. (d) Classification of symptomatic and asymptomatic grapevine leaves. Images from laboratory and field for model YOLOv5-v4. (e) Classification of laboratory and field images for model YOLOv5-v5.

A CNN model with the YOLOv5 architecture was trained using the dataset presented in Figure 9a and achieved an Accuracy of 91.41%. However, this model was limited to only detecting symptomatic and asymptomatic leaves from individual leaf images. Figure 10a illustrates the confusion matrix of the first model trained on an unbalanced dataset. In the second version of the model's dataset, the number of images in each class was balanced, with 1200 in the *asymptomatic* class and 1500 in the *symptomatic* class. By increasing the number of asymptomatic images, the model achieved better results in leaf detection, as shown in Figure 9b. However, this version could not detect leaf symptoms in field images. The results obtained from this second model version are presented in Figure 10b. This model achieved an Accuracy of 95% and could detect individual leaves exposed to artificial light, regardless of whether they exhibited symptoms. For the third version of the model, 1200 images were used in the *asymptomatic* class and 1400 in the *symptomatic* class, as depicted in Figure 9c. Unlike the previous models, the Accuracies presented in Figure 10c were validated by incorporating field images. The fourth version introduced field images, including plants with GRBD and/or GLD symptoms, to further diversify the dataset with images from the laboratory and the field. This adjustment increased the *symptomatic* class to 1600 images, while the *asymptomatic* class remained at 1200, which resulted in a critical class imbalance, as shown in Figure 9d. The model achieved an Accuracy of 96.32%, as depicted in Figure 10d. The final version of the model was developed based on the performance of the fifth YOLOv5 model, which incorporated all necessary modifications. Since the two classes were more balanced, as shown in Figure 9e, the model achieved higher and closer metrics of Precision and Recall, as illustrated in the confusion matrix in Figure 10e.

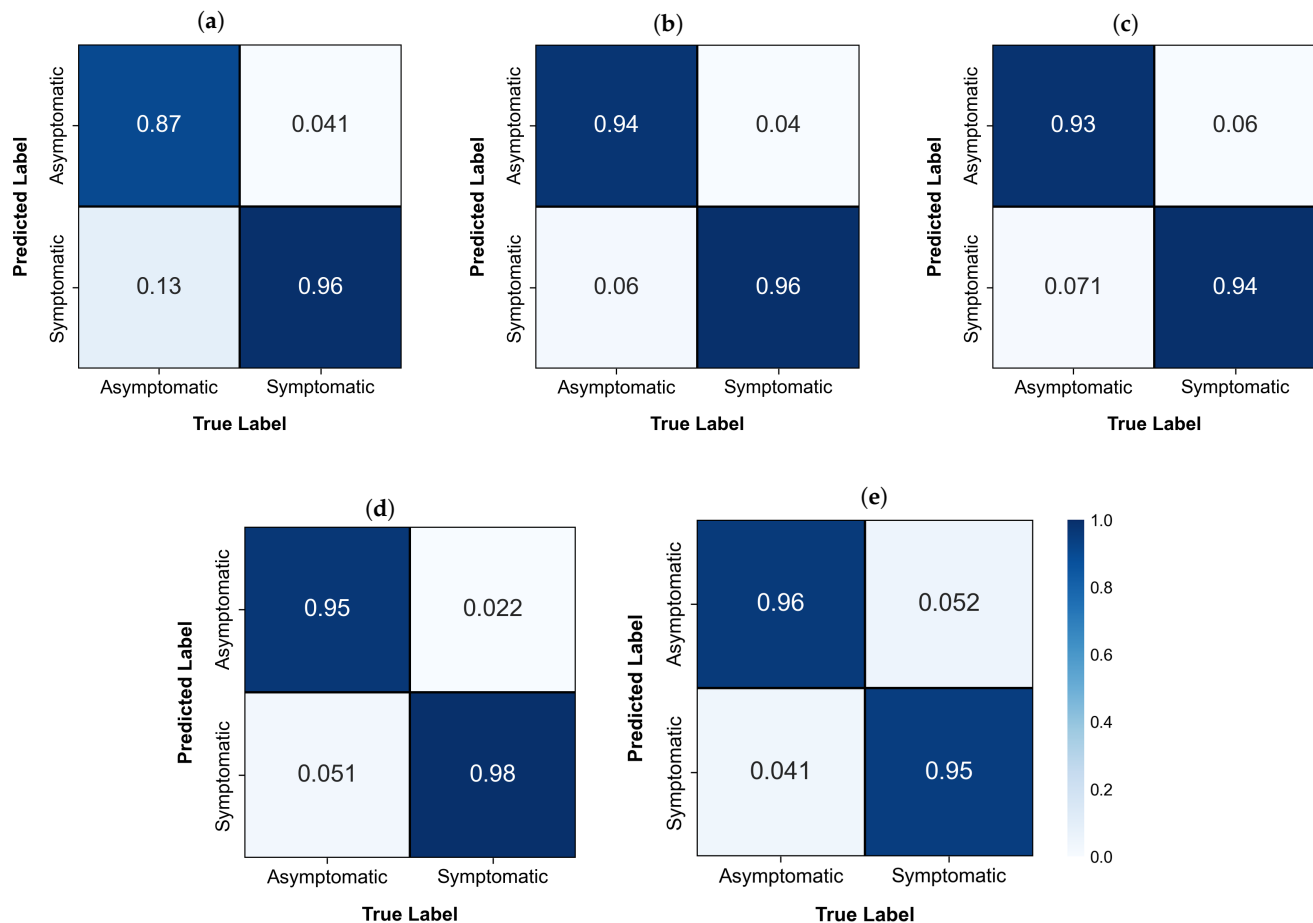


Figure 10. Confusion matrices obtained for the five trained versions of YOLOv5 with different datasets: (a) YOLOv5-v1; (b) YOLOv5-v2; (c) YOLOv5-v3; (d) YOLOv5-v4; (e) YOLOv5-v5.

Table 7 shows the classification Precision and error results per class for each of the five YOLOv5 model versions and their Accuracies. Additionally, it examines each model's capability to identify the visual features of GRBD and GLD while evaluating their performance in classifying low-resolution images.

Table 7. Metrics for YOLOv5 model varying the dataset characteristics.

Metrics	YOLOv5-v1	YOLOv5-v2	YOLOv5-v3	YOLOv5-v4	YOLOv5-v5
Asymptomatic class Precision	95.52%	95.92%	93.93%	97.76%	94.85%
Asymptomatic class error	4.48%	4.08%	6.07%	2.24%	5.15%
Symptomatic class Precision	88.06%	94.12%	92.94%	95.05%	95.87%
Symptomatic class error	11.94%	5.88%	7.06%	4.95%	4.13%
Accuracy	91.41%	95.00%	93.43%	96.37%	95.36%
Classification of individual leaves	Yes	Yes	Yes	Yes	Yes
Classification of asymptomatic grapevine leaves	No	No	Yes	Yes	Yes
Classification of symptomatic grapevine leaves	No	No	No	Yes	Yes
Classification of low-resolution images	No	No	No	No	Yes

Figure 11 illustrates the confusion matrices of the four DL models selected, as discussed in Section 3. These models were trained using the same dataset of 3198 images that achieved the highest detection results for the YOLOv5 models, as presented in Table 7. The

models used to compare the performance and identify the most effective one for detecting symptoms related to GRBD and GLD were YOLOv3, YOLOv5, YOLOv8, and ResNet-50.

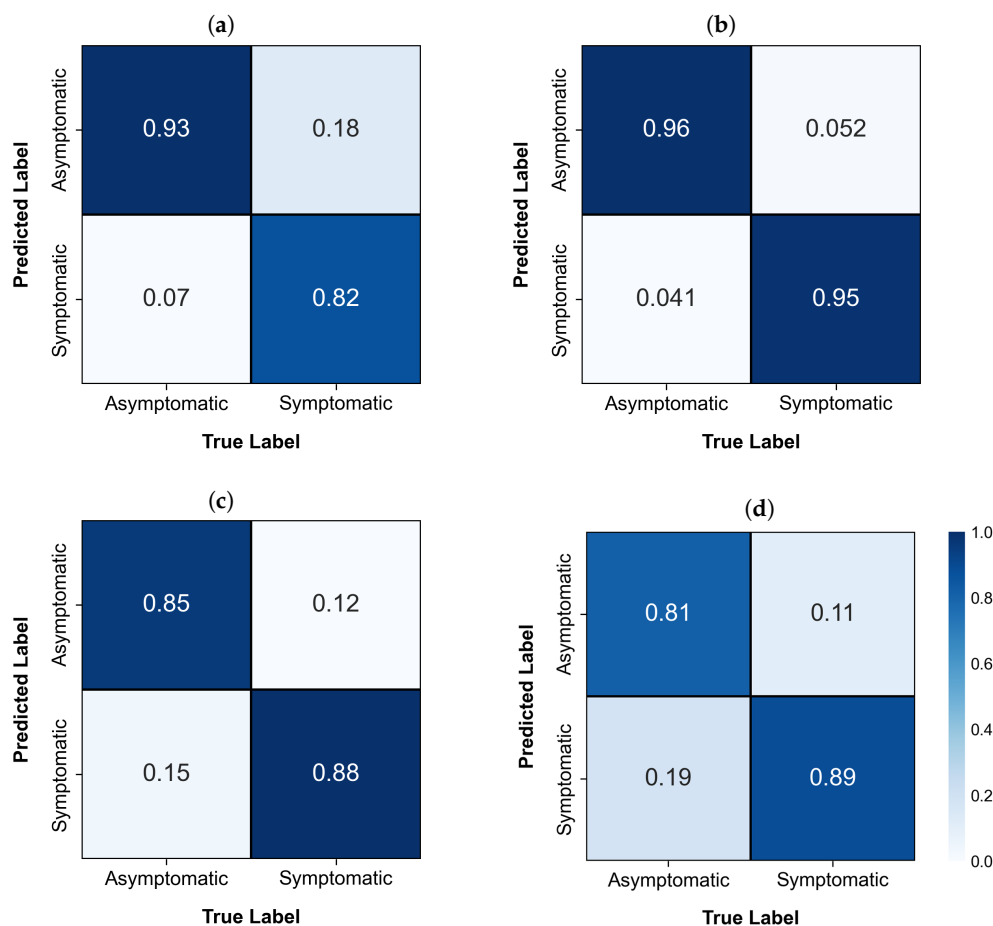


Figure 11. Confusion matrices for the trained models: (a) YOLOv3, (b) YOLOv5, (c) YOLOv8, and (d) ResNet-50.

The results obtained for the YOLOv3 model, summarized in Table 8, include an Accuracy of 87.5%, a Precision of 83.78% for the *asymptomatic* class, and 92.13% for the *symptomatic* class, as depicted in Figure 11a. Furthermore, the YOLOv5 model, presented in Figure 11, proved to be the best-performing model according to the evaluation procedure, as shown in Figure 10 and Table 7. It achieved an Accuracy of 95.36%, a Precision of 94.85% for the *asymptomatic* class, and 95.87% for the *symptomatic* class. For YOLOv8, the Accuracy was 86.5%, with a Precision of 87.63% for the *asymptomatic* class and 85.44% for the *symptomatic* class, as illustrated in Figure 11c. The confusion matrix for ResNet-50, shown in Figure 11d, reveals a lower detection rate for the *asymptomatic* class. The Accuracy of this DL model was 85.16%, with a Precision of 87.99% for the *asymptomatic* class and 82.72% for the *symptomatic* class, as detailed in Table 8.

Finally, the model with the best classification performance for the *asymptomatic* class was YOLOv5, followed by YOLOv3, YOLOv8, and ResNet-50, respectively. For the *symptomatic* class, YOLOv5 also outperformed the other models. In this case, the second-best model was ResNet-50, followed by YOLOv8 and YOLOv3. These results suggest that the YOLOv3, YOLOv8, and ResNet-50 models faced challenges in accurately detecting both classes.

The training process accounted for different field conditions, including occlusions caused by obstacles, fluctuations in light intensity across images, and overlapping leaves. Figure 12a illustrates a successful detection despite an object partially obstructing the leaves,

while Figure 12b demonstrates the model's capability to identify leaves under different lighting conditions. Similarly, Figure 12c showcases another instance of occlusion, and Figure 12d highlights a case of significant leaf overlap. The model's class confidence score ranged from 0.28 to 0.85, reflecting its ability to detect leaves under these conditions.

Table 8. Comparison of the four DL models performance metrics.

Model	Classes	Accuracy	Precision	1-Precision	Recall	1-Recall	F1-Score
YOLOv3	Asymptomatic	0.8750	0.8378	0.1622	0.9300	0.0700	0.8815
	Symptomatic		0.9213	0.0787	0.8200	0.1800	0.8677
YOLOv5	Asymptomatic	0.9536	0.9485	0.0515	0.9592	0.0408	0.9538
	Symptomatic		0.9587	0.0413	0.9479	0.0521	0.9533
YOLOv8	Asymptomatic	0.8650	0.8763	0.1237	0.8500	0.1500	0.8629
	Symptomatic		0.8544	0.1456	0.8800	0.1200	0.8670
ResNet-50	Asymptomatic	0.8516	0.8799	0.1201	0.8143	0.1857	0.8459
	Symptomatic		0.8272	0.1728	0.8889	0.1111	0.8569

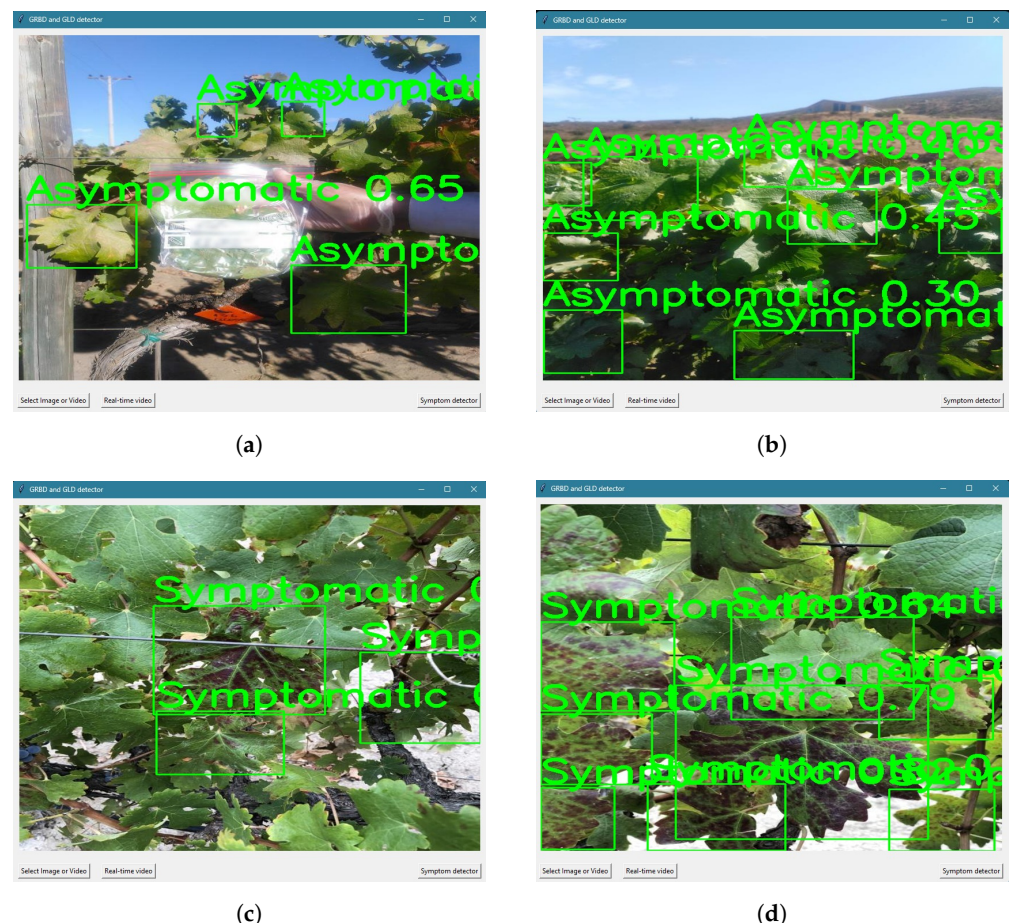


Figure 12. YOLOv5 symptoms detection results under field conditions: (a) occlusion, (b) lighting fluctuations, (c) obstacles, and (d) leaf overlapping.

Figure 13 presents the confusion matrix derived from evaluating the YOLOv5 model on a test dataset that consisted of 600 images with molecular diagnoses, with 400 symptomatic and 200 asymptomatic images, which served as the test values. The model demonstrated high Accuracy in classifying the images, where it achieved a 95% success rate for the asymptomatic class and 88% for the symptomatic class. These results highlight the model's robust capability to distinguish between the two conditions, which is critical for applications

in plant health and early symptom detection on grapevine leaves. This balance between error rates and predictive performance underscores the effectiveness of YOLOv5. These results indicate that the YOLOv5 model is well-suited for evaluating symptom detection in images, video, and real-time video in field and laboratory scenarios.

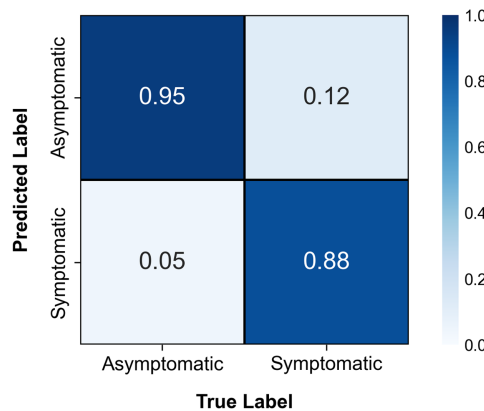


Figure 13. Confusion matrix for the test of YOLOv5 versus molecular diagnosis.

Table 9 summarizes the performance metrics of the YOLOv5 model when tested with a dataset of leaf images, comparing its predictions against molecular diagnoses as reference values. The metrics Accuracy, Precision, Recall, and F1-score provided a comprehensive evaluation of the model's predictive capabilities for both the *asymptomatic* and *symptomatic* classes. For the *asymptomatic* class, the model achieved an Accuracy of 91.25%, a Precision of 88.37%, and a Recall of 95.00%, indicating a strong performance in correctly identifying asymptomatic samples. Furthermore, the table presents the model's performance across different image resolutions (240×240 , 480×480 , and 640×640), demonstrating the effect of resolution on the classification Accuracy. At 240×240 resolution, the model achieved an Accuracy of 87.63% for asymptomatic leaves and 93.62% for symptomatic ones, with a lower Recall of 80.77% for symptomatic cases, suggesting a higher rate of false negatives. At the 480×480 resolution, the model's overall performance improved, where the Accuracy reached 91.25% for asymptomatic leaves and 94.59% for symptomatic ones. The F1-score for symptomatic classification also increased to 90.91%, reflecting a more balanced detection of diseased samples. Finally, at the 640×640 resolution, the model achieved the highest Recall (98.00% for asymptomatic and 88.00% for symptomatic samples), but with a slight trade-off in Precision, particularly for asymptomatic leaves (89.09%). These results suggest that increasing the image resolution enhanced the model's ability to detect symptomatic leaves, and thus, reduced the false negative rate. However, beyond a certain resolution, gains in performance became marginal, as observed in the small difference between the 480×480 and 640×640 results. The optimal balance between the computational efficiency and Accuracy was found at the 480×480 resolution, where the model maintained a high Precision and Recall while minimizing the computational overhead.

Table 9. Test of the YOLOv5 model with dataset images of leaves versus molecular diagnosis.

Image Resolution	Classes	Accuracy	Precision	1-Precision	Recall	1-Recall	F1-Score
240×240	Asymptomatic	0.8763	0.8309	0.1691	0.9450	0.0550	0.8843
	Symptomatic		0.9362	0.0638	0.8077	0.1923	0.8672
480×480	Asymptomatic	0.9125	0.8837	0.1163	0.9500	0.0500	0.9157
	Symptomatic		0.9459	0.0541	0.8750	0.1250	0.9091
640×640	Asymptomatic	0.9300	0.8909	0.1091	0.9800	0.0200	0.9333
	Symptomatic		0.9778	0.0222	0.8800	0.1200	0.9263

4.3. Hardware Selection

This section evaluates the hardware using the model with the best metrics for detecting symptoms in grapevine leaves and provides the necessary information for the optimal selection of hardware to deploy the model in a real-world scenario. As mentioned above, the selected hardware included two edge computing devices, namely, a Jetson Nano with 2 GB and a Raspberry Pi 4, and a high-performance computer. The model was evaluated in inference mode on a short video and in real-time vision scenarios for field deployment. The results obtained are shown in Table 10. These results demonstrate the capability of these devices at handling recordings and real-time camera input, highlighting the performance of edge computing devices compared with high-performance personal computers. In this benchmarking process, which aimed to select the appropriate hardware, the edge computing devices showed longer processing times. However, Raspberry Pi 4 is an excellent, cost-effective option for testing the YOLOv5 model. With an image resolution of 240×240 , this device can process low-resolution videos in real-time at 1.8 FPS. The Jetson Nano is a higher-performance option for processing due to its ability to handle various resolutions effectively. It can process video at approximately 4 FPS for a resolution of 240×240 , 2 FPS for 480×480 , and 1 FPS for 640×640 . These performance metrics are detailed in Table 10. Those metrics demonstrate the Jetson Nano's capability to handle images, video recordings, and real-time video across a range of resolutions in lab and field applications.

Table 10. Benchmarking of edge computing devices for AI systems and personal computer (laptop).

Edge Computing Device	Inference Time Based on Image Resolution [ms]			FPS		
	240 × 240	480 × 480	640 × 640	240 × 240	480 × 480	640 × 640
Raspberry Pi	521.4	1309.8	2160.7	1.8181	0.9012	0.5554
Jetson NANO	315.2	757.3	1277.4	3.9682	1.8181	1.0204
Personal computer (laptop)	10.4	10.4	10.5	114.9425	96.15384	78.74015

Table 10 presents the benchmarking results of three computing devices—Raspberry Pi, Jetson Nano, and a personal computer (laptop)—in terms of inference time and frames per second (FPS) for different image resolutions (240×240 , 480×480 , and 640×640). This evaluation provided insights into the performance trade-offs between edge computing devices and a high-performance computing system when deploying AI models. The benchmarking results demonstrate that while edge devices, like the Raspberry Pi and Jetson Nano, are viable options for deploying AI models, their performances varied significantly based on the computational demands of the application. The Jetson Nano offered a good balance between the cost, performance, and resolution capabilities, making it suitable for real-time tasks with moderate resolution requirements. Conversely, the personal computer's superior performance was ideal for high-throughput applications, albeit at a higher cost and reduced portability. These findings underscore the importance of selecting the appropriate hardware based on the specific requirements and constraints of the deployment scenario.

4.4. Real-World Usage Scenario

Although the system's ability to diagnose GRBD and GLD depended directly on the quality of the dataset and the inclusion of diverse images (as discussed in Section 4.1) and the performance of the model (Section 4.2), the implementation and proposed usage necessitate direct interaction between the final user and the DL model.

The process began by capturing images or videos of grapevine leaves in the field or laboratory settings. These images served as the input data for the analysis, and a camera

was used to record or capture high-quality images of the grapevine leaves. These images were then transferred to the edge computing device for further processing. The captured images were processed on an edge computing device, such as the Jetson Nano. This device executed the pre-trained YOLOv5-based DL model optimized for detecting GRBD and GLD symptoms. The processed data were visualized using custom software designed for symptom detection. The software provides the following functionalities: Image or video selection: users can select an image or video from their device for analysis. Real-time video analysis: the software supports real-time symptom detection by interfacing with live video streams. Symptom detection results: the software applies the detection model to identify symptomatic and asymptomatic areas on the leaves. The software displays the results of the analysis, including the classification of the detected areas as symptomatic or asymptomatic. A confidence score indicates the likelihood of the detected symptom; these results are visual overlays on the images or video frames, highlighting the regions of interest. This end-to-end pipeline demonstrates the practical application of AI-driven symptom detection in viticulture, enabling rapid and accurate disease diagnosis in the field or laboratory. This procedure is illustrated in Figure 14.



Figure 14. Procedure for using the GRBD and GLD symptom detection system running on the Jetson Nano edge computing device.

Figure 15 illustrates using a Python-based GUI to analyze the laboratory and field input image, video, and real-time video, and by selecting the “Symptom detector” button in the GUI, the image was processed and displayed with a diagnosis result based on the DL model.

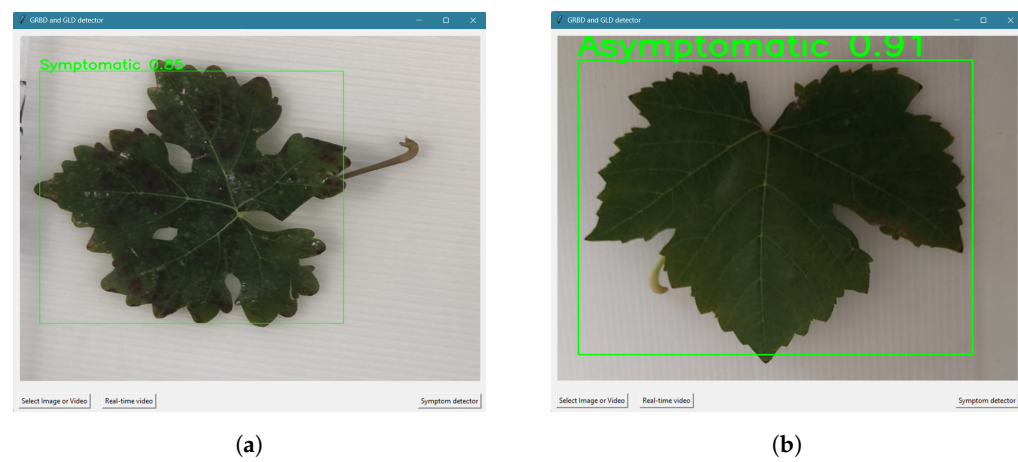


Figure 15. Cont.

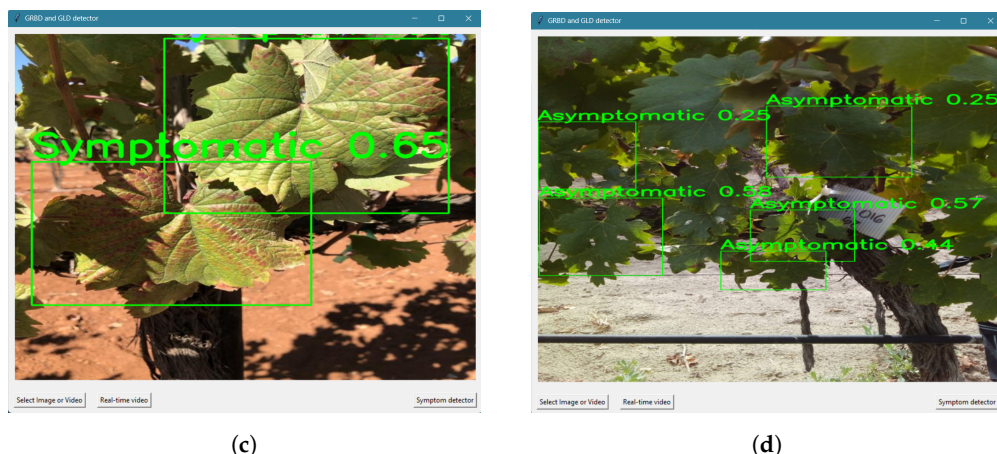


Figure 15. Graphic user interface (GUI) with classification results for (a) symptomatic laboratory image, (b) asymptomatic laboratory image, (c) symptomatic field image, and (d) asymptomatic field image.

5. Discussion

The diseases addressed in this work were GRBD and GLD, which often share symptoms, such as irregular red spots on grapevine leaves (particularly along the margins), and manifest during the same period. Other symptoms, including reddish or intense green veins, irregular edges, and leaf rolling, may also appear. Due to these viral infections, plants experience physiological and metabolic disruptions, significantly reducing the fruit quality and ripeness, resulting in economic losses for growers [20,24]. Molecular diagnostics are typically employed when GRBD and/or GLD are suspected in a vineyard. These highly sensitive techniques [41] are often expensive and require specialized personnel. Consequently, seeking alternatives, such as AI, is necessary to classify leaves showing GRBD and/or GLD symptoms, facilitating rapid and preventive diagnoses through images or serving as a preliminary measure before applying molecular diagnostic techniques.

Based on data provided by [39], information was collected in Baja California. It included symptomatic and asymptomatic grapevine leaf images with real-time RT-PCR on 800 samples with molecular diagnostics. Using this dataset, five YOLOv5 versions and four DL models were developed with various characteristics and results in terms of the evaluation metrics, including three YOLO versions (v3, v5, and v8) and ResNet-50. Comparing the YOLO and ResNet-50 versions, a higher Accuracy rate was observed with the DL models using YOLO. YOLOv5-v5 included 800 images with molecular diagnoses that categorized individual leaf and plant images, and demonstrated the ability to use low-quality images effectively for categorization.

The main differences from previously published works were the number of processed images, their quality, and the processing method. In this study, we used conventional (cellphone) cameras and 3198 images to build the dataset, and achieved an Accuracy rate of 95.36% with YOLOv5. Ref. [33] detected grape leaf diseases using various CNN and Transformer vision models, where four models achieved a 100% Accuracy, which suggests potential overfitting in the training data, leading to the memorization of examples rather than learning visual characteristics. Other studies, like [31], employed hyperspectral imaging and molecular diagnostics, such as PCR, to detect GLD and GRBV, where they achieved a 87% Accuracy with CNN models compared with 82.8% with RF models. Unlike the work by [17], which detected leafroll disease (GLRaV-3) in grapevine plants using a least squares support vector machine classifier (LS-SVM) and obtained accuracies from 66.67% to 89.93%, this study achieved higher Accuracy rates in both categories with a more straightforward approach for detecting GRBD and/or GLD. Other studies used different models or study units. Ref. [35] detected grape clusters and evaluated biophysical lesions using YOLO models (YOLOv5x6, YOLOv7-E6E, and YOLOR-CSP-X), where YOLOv7 achieved the high-

est Accuracy at 98%. Similarly, ref. [36] used improved YOLOXS (GFCD-YOLOXS) and CBAM models to identify 15 grape diseases, with an Accuracy of 99.10%. In comparison, this study identified YOLOv5 as the most effective model for leaf detection. Refs. [34,37] used the ResNet model; the former performed a quick vineyard health diagnosis based on digital images, where it obtained an F-measure of 96.6% and an intersection over the union of 93.4%, while the latter compared deep learning methods to recognize grapevine growth stages and achieved an Accuracy of 88.1%.

The presence of GRBD and GLD can vary depending on climate, grape variety, and environmental factors. Additionally, differences in lighting, soil nutrients and water availability can affect how symptoms appear, which may impact the model's Accuracy. To enhance the model's adaptability, the training dataset included images with varying lighting conditions and quality in terms of clarity and sharpness, as well as images from both the laboratory and the field, as seen in Figure 9. Consequently, the DL model test described in Section 4.3 was conducted to identify the optimal computing device for the use case, considering different image resolutions that comprised 240×240 , 480×480 , and 640×640 . This resulted in the selection of the edge computing device Jetson NANO, which reached an inference time of 1.2774 s and a frame rate of 1.0204 FPS at a resolution of 640×640 . Adapting this approach to different regions or crops comes with several challenges. Therefore, transfer learning can be used to fine-tune the model with region-specific datasets, ensuring reliable detection across various grape-growing areas. Moreover, the implementation under field conditions must consider the variability in image quality attributable to diverse devices, angles, and illumination conditions.

Based on the evaluation of three different hardware devices, the Jetson Nano was identified as the most suitable option for deploying the trained DL model in real-world agricultural scenarios. Its optimal balance between computational efficiency and portability makes it an excellent choice for edge computing applications, particularly in precision agriculture. As highlighted by [51], the Jetson Nano combination of processing power, low energy consumption and compact design enables efficient real-time disease detection in field conditions. These findings reinforce the feasibility of integrating deep learning-based disease detection into practical vineyard management strategies, paving the way for scalable and cost-effective monitoring solutions.

Finally, it is essential to consider that diagnosis based on symptoms may not reliably identify asymptomatic or virus-free plants, as some grape cultivars do not exhibit symptoms despite infection with GLD- and/or GRBD-associated viruses. Additionally, early-stage infections may also be asymptomatic [24]. Therefore, molecular diagnostics are recommended to confirm results. Notably, the presence of viruses requires molecular confirmation, as the leaf symptoms of these diseases appear only during specific and brief time windows and may also be influenced by external factors, such as nutrient deficiencies or water stress [52].

6. Conclusions

A robust database was created based on molecular diagnostics associated with symptomatic samples and images, enabling the development of an AI model informed by molecular diagnostic outcomes. DL models, such as YOLOv3, YOLOv5, YOLOv8, and ResNet-50, were assessed for their efficacy in detecting signs of grapevine red blotch disease (GRBD) and grapevine leafroll disease (GLD). The testing findings indicated that YOLOv5 outperformed the other models, with a Precision of 95.36%, Recall of 95.77%, and an F1-score of 95.56%. These data highlight the model's efficacy in precisely categorizing grapevine leaves exhibiting signs of GRBD and/or GLD and those without symptoms. A benchmarking analysis of two edge computing devices revealed that the Jetson NANO

had the most favorable cost–benefit ratio, validating the feasibility of using the proposed method in real agricultural settings. The results demonstrate that the YOLOv5-based approach is suitable for on-site vineyard monitoring, enabling rapid disease identification and response actions.

The main aim of this study was to create an enhanced DL model for the early detection of GRBD and/or GLD symptoms, allowing for timely intervention to support vineyard owners, technicians, and researchers. An intuitive interface was created to enhance the accessibility and use, enabling the rapid deployment of the proposed YOLOv5 model. The model showed proficiency in identifying symptoms in both individual leaves and whole grapevine plants, yet it is advisable to obtain close-up images of leaves to enhance the diagnostic Accuracy. This study’s results underscore YOLOv5’s potential as a strong and reliable instrument for extensive agricultural monitoring, providing substantial economic advantages via early disease diagnosis and proactive management measures.

Future Work

The main interest of this study in the future is to improve the dataset diversity to consider a broader range of environmental conditions, such as lighting, occlusions, and the presence of near objects or obstacles, as well as potential leaf conditions that could interfere with the visual diagnosis of the diseases’ symptoms, like leaf nutrient deficiencies or hydric stress. Moreover, integrating additional data sources, such as multispectral or hyperspectral imaging, could enhance the diagnostic Accuracy beyond symptom recognition. Developing a mobile application or a cloud-based system could enable real-time analysis for grapevine growers, thereby facilitating the efficient monitoring of their vineyards. Another future contribution will be to update the dataset considering additional regions in Mexico and worldwide to confirm its usability and versatility under other environmental and climatological conditions.

Author Contributions: Conceptualization, K.G.G.-R. and O.A.A.-C.; Data curation, E.I.-G. and E.E.G.-G.; Formal analysis, D.C.-V. and C.A.L.-M.; Funding acquisition, J.C.-T.; Investigation, C.L.-G. and K.G.G.-R.; Methodology, C.L.-G., O.A.A.-C. and K.G.G.-R.; Project administration, E.I.-G. and K.G.G.-R.; Resources, E.I.-G. and J.C.-T.; Software, C.L.-G., O.A.A.-C. and J.G.-F.; Supervision, E.I.-G. and E.E.G.-G.; Validation, D.C.-V., C.A.L.-M. and E.E.G.-G.; Visualization, D.C.-V. and C.A.L.-M.; Writing—original draft, C.L.-G., K.G.G.-R., J.G.-F. and O.A.A.-C.; Writing—review and editing, J.C.-T., O.A.A.-C. and E.I.-G. All authors read and agreed to the published version of this manuscript.

Funding: This research was funded by the Universidad Autónoma de Baja California (UABC) through the 25th internal call for research projects with grant number 402/6/C/53/25 and the Centro de Investigación Científica y de Educación Superior de Ensenada (CICESE, institutional project 683210). Furthermore, thanks to Comité Estatal de Sanidad Vegetal de Baja California (CESVBC) and SADERBC (Vine Phytosanitary Management Project), The authors also thank CONAHCyT with FOP02-2021-4 Grant 316602 and the scholarship awarded to K. G. García-Resendiz and J. Galarza-Falfan.

Institutional Review Board Statement: Not applicable.

Informed Consent Statement: Not applicable.

Data Availability Statement: The dataset is available at: Garcia, Karen; Carrillo Tripp, Jimena. 2024. Grapevine Virus and Symptom Database (GVS-DB), Mendeley Data, V1 at <https://doi.org/10.17632/wkbd3wsjpj.1>.

Acknowledgments: The authors would like to thank the Universidad Autónoma de Baja California and the Centro de Investigación Científica y de Educación Superior de Ensenada for the support provided in the use of the laboratories and computing equipment

Conflicts of Interest: The authors declare no conflicts of interest.

Abbreviations

The following abbreviations are used in this manuscript:

AI	Artificial intelligence
ANN	Artificial Neural Network
CBAM	Convolutional Block Attention Module
CNN	Convolutional Neural Network
DL	Deep learning
GLD	Grapevine leafroll disease
GLRaVs	Grapevine leafroll-associated viruses
GRBD	Grapevine red blotch disease
GRBV	Grapevine red blotch virus
LS-SVM	Least squares support vector machine
ML	Machine learning
RT-PCR	Reverse transcription polymerase chain reaction
ResNet	Residual network
RF	Random Forest
YOLO	You Only Look Once

References

1. Gatou, P.; Tsiora, X.; Spitalas, A.; Sioutas, S.; Vonitsanos, G. Artificial Intelligence Techniques in Grapevine Research: A Comparative Study with an Extensive Review of Datasets, Diseases, and Techniques Evaluation. *Sensors* **2024**, *24*, 6211. [[CrossRef](#)] [[PubMed](#)]
2. International Organisation of Vine and Wine. 2022. Available online: https://www.oiv.int/sites/default/files/documents/OIV_Actualidad_de_la_coyuntura_del_sector_vitivinicola_mundial_en_2022_0.pdf (accessed on 2 February 2024).
3. Cierre de la Producción Agrícola en México. 2025. Available online: <https://nube.siap.gob.mx/cierreagricola> (accessed on 9 January 2025).
4. Grape Production in Mexico 2022. Available online: <https://www.gob.mx/siap/documentos/produccion-de-uva-en-mexico-2022> (accessed on 19 December 2023).
5. Sembradas 4,365 hectáreas con vid en la Zona Costa de baja California: Agricultura. 2023. Available online: <https://www.gob.mx/agricultura/bajacalifornia/articulos/seembradas-4-365-hectareas-con-vid-en-la-zona-costa-de-baja-california-agricultura> (accessed on 29 January 2024).
6. Yepes, L.M.; Cieniewicz, E.; Krenz, B.; McLane, H.; Thompson, J.R.; Perry, K.L.; Fuchs, M. Causative Role of Grapevine Red Blotch Virus in Red Blotch Disease. *Phytopathology®* **2018**, *108*, 902–909. [[CrossRef](#)] [[PubMed](#)]
7. Gasperin-Bulbarela, J.; Licea-Navarro, A.F.; Pino-Villar, C.; Hernández-Martínez, R.; Carrillo-Tripp, J. First Report of Grapevine Red Blotch Virus in Mexico. *Plant Dis.* **2019**, *103*, 381–381. [[CrossRef](#)]
8. Krenz, B.; Fuchs, M.; Thompson, J.R. Grapevine red blotch disease: A comprehensive Q&A guide. *PLoS Pathog.* **2023**, *19*, 1–6. [[CrossRef](#)]
9. ICTV. Genus: Grablovirus. 2010. Available online: <https://ictv.global/report/chapter/geminiviridae/geminiviridae/grablovirus> (accessed on 19 December 2023).
10. Fiallo-Olivé, E.; Lett, J.M.; Martin, D.P.; Roumagnac, P.; Varsani, A.; Zerbini, F.M.; Navas-Castillo, J. ICTV Virus Taxonomy Profile: Geminiviridae 2021. *J. Gen. Virol.* **2021**, *102*, 001696. [[CrossRef](#)] [[PubMed](#)]
11. Fuchs, M.; Bar-Joseph, M.; Candresse, T.; Maree, H.J.; Martelli, G.P.; Melzer, M.J.; Menzel, W.; Minafra, A.; Sabanadzovic, S.; ICTV Report Consortium. ICTV Virus Taxonomy Profile: Closteroviridae. *J. Gen. Virol.* **2020**, *101*, 364–365. [[CrossRef](#)]
12. Hommay, G.; Beuve, M.; Herrbach, E. Transmission of Grapevine Leafroll-Associated Viruses and Grapevine Virus A by Vineyard-Sampled Soft Scales (*Parthenolecanium corni*, Hemiptera: Coccoidea). *Viruses* **2022**, *14*, 2679. [[CrossRef](#)]
13. Cabaleiro, C.; Pesqueira, A.M.; Segura, A. Planococcus ficus and the spread of grapevine leafroll disease in vineyards: A 30-year-long case study in north-West Spain. *Eur. J. Plant Pathol.* **2022**, *163*, 733–747. [[CrossRef](#)]
14. Comité Estatal de Sanidad Vegetal de Baja California. Plagas de vid. 2023. Available online: <https://www.cesvbc.org/copia-de-manejo-fitosanitario-de-fr> (accessed on 29 January 2024).
15. Herrbach, E.; Alliaume, A.; Prator, C.A.; Daane, K.M.; Cooper, M.L.; Almeida, R.P.P. Vector Transmission of Grapevine Leafroll-Associated Viruses. In *Grapevine Viruses: Molecular Biology, Diagnostics and Management*; Springer International Publishing: Cham, Switzerland, 2017; pp. 483–503. [[CrossRef](#)]

16. Atallah, S.S.; Gómez, M.I.; Fuchs, M.F.; Martinson, T.E. Economic Impact of Grapevine Leafroll Disease on *Vitis vinifera* cv. Cabernet franc in Finger Lakes Vineyards of New York. *Am. J. Enol. Vitic.* **2012**, *63*, 73–79. [CrossRef]
17. Gao, Z.; Khot, L.R.; Naidu, R.A.; Zhang, Q. Early detection of grapevine leafroll disease in a red-berried wine grape cultivar using hyperspectral imaging. *Comput. Electron. Agric.* **2020**, *179*, 105807. [CrossRef]
18. Burger, J.T.; Maree, H.J.; Gouveia, P.; Naidu, R.A. Grapevine leafroll-associated virus3. In *Grapevine Viruses: Molecular Biology, Diagnostics and Management*; Springer International Publishing: Cham, Switzerland, 2017; pp. 167–195. [CrossRef]
19. Bahder, B.W.; Zalom, F.G.; Jayanth, M.; Sudarshana, M.R. Phylogeny of Geminivirus Coat Protein Sequences and Digital PCR Aid in Identifying *Spissistilus festinus* as a Vector of Grapevine red blotch-associated virus. *Phytopathology®* **2016**, *106*, 1223–1230. [CrossRef] [PubMed]
20. Blanco-Ulate, B.; Hopfer, H.; Figueroa-Balderas, R.; Ye, Z.; Rivero, R.M.; Albacete, A.; Pérez-Alfocea, F.; Koyama, R.; Anderson, M.M.; Smith, R.J.; et al. Red blotch disease alters grape berry development and metabolism by interfering with the transcriptional and hormonal regulation of ripening. *J. Exp. Bot.* **2017**, *68*, 1225–1238. [CrossRef] [PubMed]
21. Rumbaugh, A.C.; Sudarshana, M.R.; Oberholster, A. Grapevine Red Blotch Disease Etiology and Its Impact on Grapevine Physiology and Berry and Wine Composition. *Horticulturae* **2021**, *7*, 552. [CrossRef]
22. Ricketts, K.D.; Gómez, M.I.; Fuchs, M.F.; Martinson, T.E.; Smith, R.J.; Cooper, M.L.; Moyer, M.M.; Wise, A. Mitigating the Economic Impact of Grapevine Red Blotch: Optimizing Disease Management Strategies in U.S. Vineyards. *Am. J. Enol. Vitic.* **2017**, *68*, 127–135. [CrossRef]
23. Sudarshana, M.R.; Perry, K.L.; Fuchs, M.F. Grapevine Red Blotch-Associated Virus, an Emerging Threat to the Grapevine Industry. *Phytopathology®* **2015**, *105*, 1026–1032. [CrossRef] [PubMed]
24. Lee, L.; Reynolds, A.; Lan, Y.; Meng, B. Identification of unique electromagnetic signatures from GLRaV-3 infected grapevine leaves in different stages of virus development. *Smart Agric. Technol.* **2024**, *8*, 100464. [CrossRef]
25. Calvi, B.L. Effects of Red-leaf Disease on Cabernet Sauvignon at the Oakville Experimental Vineyard and Mitigation by Harvest Delay and Crop Adjustment. Master’s Thesis, University of California, Davis, CA, USA, 2011.
26. Krenz, B.; Thompson, J.R.; McLane, H.L.; Fuchs, M.; Perry, K.L. Grapevine red blotch-associated virus Is Widespread in the United States. *Phytopathology®* **2014**, *104*, 1232–1240. [CrossRef] [PubMed]
27. Naidu, R.A.; Maree, H.J.; Burger, J.T. Grapevine Leafroll Disease and Associated Viruses: A Unique Pathosystem. *Annu. Rev. Phytopathol.* **2015**, *53*, 613–634. [CrossRef] [PubMed]
28. Naidu, R.; Rowhani, A.; Fuchs, M.; Golino, D.; Martelli, G.P. Grapevine Leafroll: A Complex Viral Disease Affecting a High-Value Fruit Crop. *Plant Dis.* **2014**, *98*, 1172–1180. [CrossRef]
29. Martelli, G. Directory of virus and virus-like diseases of the grapevine and their agents. *J. Plant Pathol.* **2014**, *96*, 1–136.
30. Sekharantry, P.K.; Rao, M.S.; Srinivas, Y.; Uriti, A. PSR-LeafNet: A Deep Learning Framework for Identifying Medicinal Plant Leaves Using Support Vector Machines. *Big Data Cogn. Comput.* **2024**, *8*, 176. [CrossRef]
31. Sawyer, E.; Laroche-Pinel, E.; Flasco, M.; Cooper, M.L.; Corrales, B.; Fuchs, M.; Brillante, L. Phenotyping grapevine red blotch virus and grapevine leafroll-associated viruses before and after symptom expression through machine-learning analysis of hyperspectral images. *Front. Plant Sci.* **2023**, *14*, 1117869. [CrossRef] [PubMed]
32. Maeda Gutiérrez, V.; Guerrero Méndez, C.; Olvera Olvera, C.A.; Araiza Esquivel, M.A.; Espinoza García, G.; Bordón López, R. Convolutional neural networks for detection and classification of plant diseases based on digital imagenes. *Rev. BiolóGico Agropecu. Tuxpan* **2018**. [CrossRef]
33. Kunduracioglu, I.; Pacal, I. Advancements in deep learning for accurate classification of grape leaves and diagnosis of grape diseases. *J. Plant Dis. Prot.* **2024**, *131*, 1061–1080. [CrossRef]
34. Elsherbiny, O.; Elaraby, A.; Alahmadi, M.; Hamdan, M.; Gao, J. Rapid Grapevine Health Diagnosis Based on Digital Imaging and Deep Learning. *Plants* **2024**, *13*, 135. [CrossRef] [PubMed]
35. Pinheiro, I.; Moreira, G.; Queirós da Silva, D.; Magalhães, S.; Valente, A.; Moura Oliveira, P.; Cunha, M.; Santos, F. Deep Learning YOLO-Based Solution for Grape Bunch Detection and Assessment of Biophysical Lesions. *Agronomy* **2023**, *13*, 1120. [CrossRef]
36. Wang, C.; Wang, Y.; Ma, G.; Bian, G.; Ma, C. Identification of Grape Diseases Based on Improved YOLOXS. *Appl. Sci.* **2023**, *13*, 5978. [CrossRef]
37. Schieck, M.; Krajsic, P.; Loos, F.; Hussein, A.; Franczyk, B.; Kozierkiewicz, A.; Pietranik, M. Comparison of deep learning methods for grapevine growth stage recognition. *Comput. Electron. Agric.* **2023**, *211*, 107944. [CrossRef]
38. Foundation Plant Services, UC Davis. FPS Grape Program—Sample Collection. 2025. Available online: <http://fps.ucdavis.edu/samplecollection.cfm> (accessed on 24 January 2025).
39. García, K.; Carrillo Tripp, J. Grapevine Virus and Symptom Database (GVS-DB); Mendeley Data, 2024. Available online: <https://data.mendeley.com/datasets/wkbd3wsjpj/1> (accessed on 5 December 2025).
40. Gambino, G.; Perrone, I.; Gribaudo, I. A Rapid and effective method for RNA extraction from different tissues of grapevine and other woody plants. *Phytochem. Anal.* **2008**, *19*, 520–525. [CrossRef]

41. Osman, F.; Leutenegger, C.; Golino, D.; Rowhani, A. Real-time RT-PCR (TaqMan) assays for the detection of Grapevine Leafroll associated viruses 1-5 and 9. *J. Virol. Methods* **2007**, *141*, 22–29. [[CrossRef](#)]
42. Jocher, G. YOLOv5 by Ultralytics. 2020. [[CrossRef](#)]
43. Liu, H.; Sun, F.; Gu, J.; Deng, L. SF-YOLOv5: A Lightweight Small Object Detection Algorithm Based on Improved Feature Fusion Mode. *Sensors* **2022**, *22*, 5817. [[CrossRef](#)]
44. Ultralytics. Data Augmentation—Tools and Libraries. 2024. Available online: <https://www.ultralytics.com/glossary/data-augmentation#tools-and-libraries> (accessed on 18 January 2024).
45. Redmon, J.; Farhadi, A. YOLOv3: An Incremental Improvement. *arXiv* **2018**. [[CrossRef](#)]
46. Reis, D.; Kupec, J.; Hong, J.; Daoudi, A. Real-Time Flying Object Detection with YOLOv8. *arXiv* **2023**. [[CrossRef](#)]
47. Jocher, G.; Chaurasia, A.; Qiu, J. Ultralytics YOLOv8. 2023. . . [[CrossRef](#)]
48. He, K.; Zhang, X.; Ren, S.; Sun, J. Deep Residual Learning for Image Recognition. *arXiv* **2015**. [[CrossRef](#)]
49. Bendjillali, R.I.; Beladgham, M.; Merit, K.; Taleb-Ahmed, A. Illumination-robust face recognition based on deep convolutional neural networks architectures. *Indones. J. Electr. Eng. Comput. Sci.* **2020**, *18*, 1015–1027. [[CrossRef](#)]
50. Dwyer, B.; Nelson, J.; Hansen, T. Roboflow (Version 1.0) [Software]. 2024. Available online: <https://roboflow.com> (accessed on 18 January 2024).
51. Galarza-Falfan, J.; García-Guerrero, E.E.; Aguirre-Castro, O.A.; López-Bonilla, O.R.; Tamayo-Pérez, U.J.; Cárdenas-Valdez, J.R.; Hernández-Mejía, C.; Borrego-Dominguez, S.; Inzunza-Gonzalez, E. Path Planning for Autonomous Mobile Robot Using Intelligent Algorithms. *Technologies* **2024**, *12*, 82. [[CrossRef](#)]
52. Ju, Y.L.; Yue, X.F.; Zhao, X.F.; Zhao, H.; Fang, Y.L. Physiological, micro-morphological and metabolomic analysis of grapevine (*Vitis vinifera* L.) leaf of plants under water stress. *Plant Physiol. Biochem.* **2018**, *130*, 501–510. [[CrossRef](#)] [[PubMed](#)]

Disclaimer/Publisher’s Note: The statements, opinions and data contained in all publications are solely those of the individual author(s) and contributor(s) and not of MDPI and/or the editor(s). MDPI and/or the editor(s) disclaim responsibility for any injury to people or property resulting from any ideas, methods, instructions or products referred to in the content.